Scripta Materialia 139 (2017) 34–38

Contents lists available at ScienceDirect

Scripta Materialia

journal homepage: www.elsevier.com/locate/scriptamat

Regular article

Improving creep property of Mg–Gd–Zn alloy via trace Ca addition

C. Xu [a,b,*], T. Nakata [a,b], K. Oh-ishi [a,b], T. Homma [a,b], T. Ozaki [c], S. Kamado [a,b]

[a] Department of Mechanical Engineering, Nagaoka University of Technology, Nagaoka 940-2188, Japan
[b] Research Center for Advanced Magnesium Technology, Nagaoka University of Technology, Nagaoka 940-2188, Japan
[c] Materials Department Research Laboratory, IHI Corporation, Yokohama 235-8501, Japan

ARTICLE INFO

Article history:
Received 8 May 2017
Received in revised form 8 June 2017
Accepted 11 June 2017
Available online xxxx

Keywords:
Magnesium alloys
Creep
Precipitation
Transmission electron microscopy

ABSTRACT

Only trace Ca addition to the Mg–2Gd–0.5Zn–0.2Zr (at.%) alloy leads to the precipitation of Guinier-Preston (GP) zones and remarkably improves the creep resistance at elevated temperatures. The Mg–2Gd–0.5Zn–0.4Ca–0.2Zr alloy exhibits a minimum creep rate of 5.75×10^{-8} s^{-1} tested at 250 °C and 110 MPa, its superior creep resistance is attributed to the precipitation of dense GP zones on the basal plane, increment in number density of refined β phases on the prismatic plane of the α-Mg matrix, narrow precipitate free zones (PFZs) and strengthened long period stacking ordered (LPSO) phases by trace concentration of Ca.

The rare earth (RE)-containing Mg alloys are promising candidates in the aerospace and automobile industries due to their high specific strength and splendid thermal stability [1–3]. Because of the high solid solubility of Gd and precipitation of metastable β′ phase with base centered orthorhombic (bco) structure during ageing treatment, Mg–Gd based alloys exhibit outstanding tensile properties and superior creep resistance even compared with commercial heat resistant WE54 and QE22 alloys [4–6]. Moreover, the addition of Zn to the Mg–Gd alloys gives rise to the long period stacking ordered (LPSO) phase [7–10]. These LPSO phases raise the critical resolved shear stress (CRSS) for the basal slip and the non-basal slip in the matrix is activated so that both the strength and ductility are improved simultaneously [8]. Meanwhile, the α-Mg matrix can transfer part of its load to the LPSO phase during the creep test [9] and even if microcracking occurs at the interface between α-Mg and LPSO phase, the LPSO phase could inhibit the propagation of the microcracks by kink deformation to avoid macro fracture of the sample [10]. Nie et al. [11,12] found that the Zn addition to the Mg–Gd alloy with Zn/Gd ratio of >0.4 enhances the age hardening response and the creep strength by the homogeneous and dense distribution of basal plate-shaped precipitates, however, at the expense of the absence of any prismatic precipitates such as β′, β_1 and β phases. It is well known that the addition of Ca with low cost to Mg alloys can decrease the flammability of molten Mg alloys and make them safe for use at elevated temperatures [13]. Furthermore, it is reported that the Ca addition to Mg–Zn based alloys leads to a substantial increase in the age-hardening response and creep resistance by the precipitation of nanoscale monolayer Guinier-Preston (GP) zones on basal planes of α-Mg matrix [14,15]. The Ca addition to Mg–Gd–Zn based alloys has also been reported recently [16–18], however, whether the Ca addition affects the age-hardening response and the precipitation behavior during ageing treatment has not been analyzed so far.

In order to achieve high strength and heat resistance by the simultaneous formation of fine plate-shaped precipitates in prismatic and basal habit planes [19], in this study, Ca with contents of 0–0.4at% was added to the Mg–2.0Gd–0.5Zn–0.2Zr (all concentration in at.%, unless otherwise stated) alloy and the age-hardening response, creep resistance and corresponding microstructures were investigated.

Mg–2.0Gd–0.5Zn–xCa-0.2Zr (x = 0, 0.1, 0.2 and 0.4) alloy ingots were fabricated by permanent mould casting and they are denoted as 0Ca, 0.1Ca, 0.2Ca and 0.4Ca, respectively. The alloy compositions are listed in atom percent in Table 1. The samples for Vickers hardness test and microstructure observation were cut from the ingots and solution treated at 475 °C for 8 h in a Pyrex tube under an Ar atmosphere followed by an immediate warm water quenching. Then the solution treated samples were subjected to ageing treatment in an oil bath at 200 °C for various periods of time. Vickers hardness was measured by VMT-7S with a 5 kgf load and a holding time of 15 s. Flat specimens with a gauge length of 50 mm and cross-sectional dimension of 10×5 mm^2 were prepared and peak-aged at 200 °C prior to tensile creep test. The tensile creep test was performed using an A&D CP-6L-500 machine at temperature of 250 °C and an applied stress of 110 MPa. The temperature was maintained at ±2 °C.

The microstructure of the alloys was observed by Olympus BX60M optical microscope (OM), JEOL JEM-2100F transmission electron microscope (TEM) and high angle annular dark field (HAADF) operating at 200 kV. Thin foils for transmission electron microscope (TEM)

* Corresponding author at: Department of Mechanical Engineering, Nagaoka University of Technology, Nagaoka 940-2188, Japan.
E-mail address: xuchao@vos.nagaokaut.ac.jp (C. Xu).

http://dx.doi.org/10.1016/j.scriptamat.2017.06.012
1359-6462/

Table 1
Chemical compositions of the alloys (at.%).

Alloy	Gd	Zn	Zr	Ca	Mg
0Ca	1.99	0.53	0.16	–	Bal.
0.1Ca	2.09	0.53	0.16	0.10	Bal.
0.2Ca	2.09	0.53	0.16	0.19	Bal.
0.4Ca	2.15	0.53	0.15	0.41	Bal.

observation with thickness of 0.2 mm were punched into discs with 3 mm in diameter and mechanically polished followed by low angle ion milling using Gatan precision ion polishing system.

Fig. 1a shows the age-hardening curves of the alloys during isothermal ageing at 200 °C. As can be seen, the Ca addition brings an increase in the as-quenched hardness and all of the alloys show considerable age hardening responses. The hardness of the 0Ca increases slowly at the early stage of ageing, then sharply rises after 8 h ageing and reaches a peak of 101 HV at about 128 h, followed by a gradual decrease. The Ca containing alloys show a similar ageing behavior and a slightly shorter peak ageing time for about 64 h. The peak hardness increases with increasing Ca content and that of the 0.4Ca reaches 108 HV. It should be noted that the Ca containing alloys, especially the 0.4Ca, exhibit higher hardness than that of the 0Ca for all the ageing times.

Fig. 1b shows the creep curves obtained from peak-aged samples measured at 250 °C and 110 MPa. Remarkable improvement in the creep resistance can be observed by adding only 0.1–0.4% Ca to the Mg–Gd–Zn–Zr alloy. In analogy to the age hardening curves, the creep resistance also rises with increasing Ca content. The minimum creep rate ($\dot{\varepsilon}$) calculated from Fig. 1b is 1.99×10^{-7} s^{-1} in the 0Ca, 1.23×10^{-7} s^{-1}, 9.55×10^{-8} s^{-1} and 5.75×10^{-8} s^{-1} in the 0.1Ca, 0.2Ca and 0.4Ca, respectively. Thus the 0.4Ca shows far superior creep performance with a reduction in the $\dot{\varepsilon}$ by approximately a factor of four compared with that in the 0Ca. In comparison with T6 treated commercial WE43 alloy with $\dot{\varepsilon}$ of ~1.0×10^{-6} s^{-1} tested at 250 °C and 100 MPa [20], the $\dot{\varepsilon}$ of 0.4Ca tested at higher stress in this study is only 1/17 of that for WE43. Furthermore, only trace Ca addition makes 0.4Ca show higher creep resistance than other Mg–Gd based alloys [20,21]. It is reported that Zn addition to the Mg–Gd–Zr alloy significantly improves the creep property by basal plate precipitates at 200 °C and 90 MPa [14], nevertheless it is noteworthy that the 0.4Ca in this study exhibits superior creep resistance even examined at more severe conditions with a higher temperature of 250 °C and a higher stress of 110 MPa. The $\dot{\varepsilon}$ as a function of the applied stress at 250 °C was plotted in Fig. 1c to calculate the stress exponent (n) for analyzing the creep mechanism. It can be seen that n values of all the samples range from 5.7 to 7.4, suggesting that the dislocation creep is the dominant mechanism for all the samples despite of Ca addition [21].

In order to reveal the strengthening mechanism by Ca addition, TEM observations of the precipitates in the peak-aged 0Ca and 0.4Ca were carried out along both a and c axes of the α-Mg matrix, i.e. $[10\bar{1}0]_\alpha$, $[11\bar{2}0]_\alpha$ and $[0001]_\alpha$. Fig. 2a and b show the TEM bright field (BF) images and corresponding selected area electron diffraction (SAED) patterns with electron beam parallel to the $[0001]_\alpha$ of the peak-aged alloys. It can be seen that plate-shaped precipitates form on the prismatic planes and distribute with three variants in both alloys. According to the SAED pattern, the precipitates are determined to be β′ phases (Mg_5Gd, bco structure, $a = 2 \times a_{\alpha\text{-Mg}} \approx 0.64$ nm, $b = 8 \times d(\bar{1}100)_{\alpha\text{-Mg}} \approx 2.22$ nm, $c = c_{\alpha\text{-Mg}} \approx 0.52$ nm) [22]. At the mean time, in order to minimize the shear strain around the β′ phases, rhombic β_1 phases (Mg_3Gd, fcc structure, $a = 0.74$ nm [23]) invariably precipitate with their ends, but not the broad surfaces, attach to the β′ phases as shown in Fig. 2a [1]. When observed from $[11\bar{2}0]_\alpha$ and $[10\bar{1}0]_\alpha$, as shown in Fig. 2c–f, lamellar-shaped phases can be observed in addition to the β′ phases on the prismatic planes of both 0Ca and 0.4Ca, which are determined to be 14H LPSO phase (hexagonal, $a = 1.11$ nm $c = 3.66$ nm) [24] by the corresponding SAED pattern.

Fig. 2b clearly reveals the refinement of the β′ and β_1 phases by the 0.4% Ca addition, which definitely increases the number density of prismatic precipitates arraying on the basal plane and pin the basal gliding dislocations more effectively than those in the 0Ca. In addition to the 14H LPSO phases on basal planes, it is noted that TEM BF images of the 0.4Ca viewed from $[11\bar{2}0]_\alpha$ and $[10\bar{1}0]_\alpha$ (Fig. 2d and f) indicate the formation of thin nanoscale plate-shaped precipitates on basal planes by the addition of 0.4% Ca, the corresponding SAED patterns given in Fig. 2b and f show that extra diffraction spots and streaks appear at the positions of $1/3(11\bar{2}0)_\alpha$ and $2/3(11\bar{2}0)_\alpha$ of α-Mg matrix along $[0001]_\alpha$ direction as marked by yellow arrows in Fig. 2b and f, which prove that these thin plate-shaped precipitates on the basal plane should be Guiner-Preston (GP) zones, just like those reported in the Mg–Zn–Ca and Mg–Zn–Gd alloys [12,15,25]. Because the atomic radius of Zn (0.148 nm) is smaller than that of Mg, and the large lattice misfit caused by the oversized Gd, especially Ca atoms, and undersized Zn atoms may promote the formation of nanoscale GP zones on the basal plane to lower the system energy [15]. Saito et al. [25] analyzed the phase transformation of Mg–Gd–Zn alloys with different Gd/Zn ratios and they concluded that when Gd/Zn ratio ranges between 1 and 1.5, GP zones become dominant precipitates; when increasing the ratio to 2, GP zones coexist with the β′ phases; further increasing the ratio, β′ phases become dominant rather than GP zones. It should be mentioned that the Gd/Zn ratio of the base alloy in this study is as large as 4, so no GP zone is observed in the base alloy. However, it is worthy to mention that the compositions of undissolved Mg_3Gd phases in 0Ca and 0.4Ca were measured to be Mg–20.7% Gd–9.6% Zn–0% Zr and Mg-13.9% Gd–3.4% Zn–0% Zr–2.7% Ca, respectively. In comparison with the Mg_3Gd phase in 0Ca, it means that ~1/3 of Gd and ~2/3 of Zn atoms in the Mg_3Gd phase release to the α-Mg matrix in 0.4Ca. This difference will vary the Gd/Zn ratio in α-Mg matrix. As a result, only the 0.4%

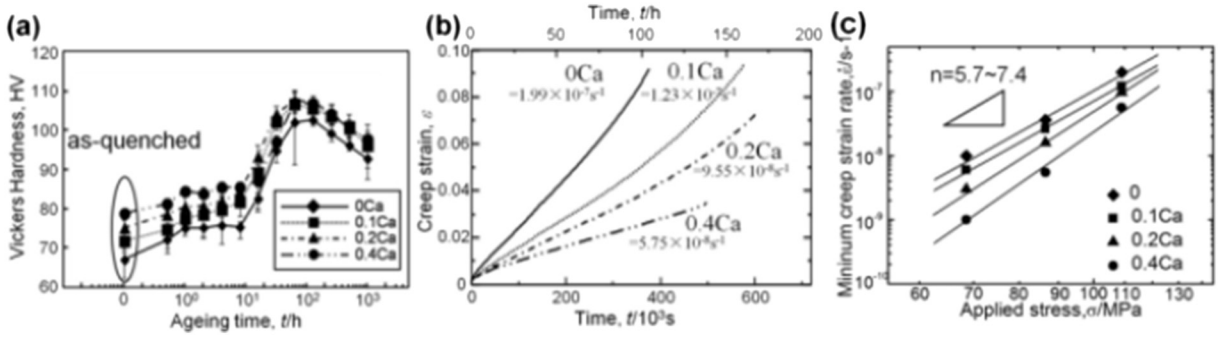

Fig. 1. (a) age-hardening curves and (b) creep curves taken from the 0Ca, 0.1Ca, 0.2Ca and 0.4Ca alloys examined at 250 °C/110 MPa, (c) Minimum creep strain rate plotted as a function of applied stress tested at 250 °C.